Combined UHV/high-pressure catalysis setup for depth-resolved near-surface spectroscopic characterization and catalytic testing of model catalysts

Lukas Mayr[1], Raffael Rameshan[1,2], Bernhard Klötzer[1], Simon Penner[1], Christoph Rameshan[1,3]

[1]*Institute of Physical Chemistry, University of Innsbruck, Innrain 52a, 6020 Innsbruck, Austria*

[2]*Department of Inorganic Chemistry, Fritz Haber Institute of the Max Planck Society, Faradayweg 4-6, 14195 Berlin, Germany*

[3]*Institute of Materials Chemistry, Vienna University of Technology, Getreidemarkt 9/BC/01, 1060 Vienna, Austria*

Abstract

An ultra-high vacuum (UHV) setup for "real" and "inverse" model catalyst preparation, depth-resolved near-surface spectroscopic characterization and quantification of catalytic activity and selectivity under technologically relevant conditions is described. Due to the all-quartz reactor attached directly to the UHV-chamber, transfer of the catalyst for in-situ testing without intermediate contact to the ambient is possible. The design of the UHV-compatible re-circulating batch reactor setup allows the study of reaction kinetics under close to technically relevant catalytic conditions up to 1273 K without contact to metallic surfaces except those of the catalyst itself. With the attached differentially pumped exchangeable evaporators and the quartz-microbalance thickness monitoring equipment, a reproducible, versatile and standardised sample preparation is possible. For three-dimensional near-surface sample characterization, the system is equipped with a hemispherical analyser for X-ray photoelectron spectroscopy (XPS), electron-beam or X-ray-excited Auger-electron spectroscopy (AES) and low-energy ion scattering (LEIS) measurements. Due the dedicated geometry of the X-ray gun (54.7°, "magic angle") and the rotatable sample holder, depth analysis by angle-resolved XPS measurements can be performed. Thus, by the combination of characterisation methods with different information depth, a detailed three-dimensional picture of the electronic and geometric structure of the model catalyst can be obtained.

To demonstrate the capability of the described system, comparative results for depth-resolved sample characterization and catalytic testing in methanol steam reforming (MSR) on PdGa and PdZn near-surface intermetallic phases (NSIP) are shown.

Introduction

A wide variety of heterogeneous catalytic reactions are performed on (bi)metal or (bi)metal/metal oxide based catalysts[1, 2]. Especially for the metal/metal oxide systems with variable interfacial regions, little is known about the local promotion of crucial elementary steps of a given reaction mechanism on the atomic scale, e.g. at phase boundary sites. To gain more knowledge about the mechanistic role of specific active sites, a better understanding of surface reactions and reactions at intermetallic surface sites or the metal-oxide interface region is hence required. An indispensable step for this goal is the standardised and reproducible preparation of "real" (i.e. metal-on-oxide) and "inverse" (i.e. oxide-on-metal) model catalysts with defined structure and composition with respect to potential active sites. A rapidly increasing number of surface science studies[3-7] reflects the actuality of this research, that has been initiated and influenced for years by the groups of Somorjai et al.[8], Hayek et al.[9], Goodman et al.[10] and Ertl et al.[11]. The second step is the systematic testing of the different model catalysts at higher pressures, i.e. under conditions similar to technical catalytic reactions. This combination of catalyst preparation and testing allows the study of the dependence of catalytic activity and selectivity on (near-)surface stoichiometry, electronic and geometric (near-)surface structure and surface defects.

A great number of model catalyst studies deal with supported materials and are therefore susceptible to metal-support interactions[12, 13]. These interactions are confined to the direct boundary between the metal and support. For a detailed investigation of metal-support interactions, the described UHV-system offers the possibility to study noble metal-oxide combinations in different ways, either as thin oxide layer(s) or as oxide islands deposited on a metal surface (inverse model catalyst) or as metal layer(s) or metal particles on an oxide surface (real model catalysts). Furthermore, surface alloys/intermetallic compounds with defined thickness and composition can be prepared[14]. With a combined study of real and

3

inverse systems and their associated catalytic performance, the influence of the interfacial regions on catalytic activity and selectivity can be studied.

With depth-resolved near-surface analysis approach, structural changes and deactivation processes on the catalyst near-surface region occurring during catalytic reactions can be detected. Furthermore, the well-known "pressure" and "materials" gaps can be studied by this combination of UHV and high-pressure studies. Especially in combination with additional in-situ XPS studies using tuneable synchrotron radiation, a clear model of the catalytic mechanism can be obtained[14, 15].

Experimental

A. General considerations

In the following sections, we describe in detail the setup of the UHV preparation and analysis chamber that is equipped with a hemispherical analyser for X-ray photoelectron spectroscopy (XPS), Auger electron spectroscopy (AES) and low-energy ion scattering (LEIS) for spectroscopic characterization. Due to the geometry of X-ray gun and hemispherical analyser and the rotatable sample holder, angle-resolved XPS measurements can be performed. A energy-variable electron gun offers to some extent the possibility to vary the kinetic energy of the primary electrons for AES measurements with consequently different analysing depth. Excitation for AES can also be performed with the X-ray gun. The ion gun of the LEIS setup can be utilized for obtaining "in-situ" sputter profiles by operation with different noble gases and higher acceleration voltages.

Depth resolved sample characterization is achieved by two ways, either by angle dependent measurements through variation of the angle between analyser and sample, or by the use of the three different methods XPS, AES and LEIS with different information depth, respectively.

Figure 1 illustrates the depth-dependent probability of no-loss escapes of photoelectrons (XPS and AES) for different analysis angles between spectrometer and sample surface. For the calculation of the plots the following equation was used:

$$P = e^{-\frac{d}{\lambda \cos \theta}}$$ (1)

P denotes the probability of photoelectrons to escape without loss at the probe depth for this probability and Θ is the take-off angle. For Auger spectroscopy measurements with the electron beam, a "reduced" EAL (effective attenuation length) for the calculation is used. This is needed because also the incident electrons are attenuated when they are penetrating the surface:

$$EAL = \frac{EAL_{e^-} \times EAL_{photo\ e^-}}{EAL_{e^-} + EAL_{photo\ e^-}}$$ (2)

For calculations of EAL the NIST database 82 version 1.3 was used (http://www.nist.gov/srd/nist82.cfm). Figure 1 clearly shows how the analysis depth varies by carrying out either XPS or Auger spectroscopy in the e-beam or X-ray mode. Combination of these measurements already at this stage allows steering the information depth at the sample.
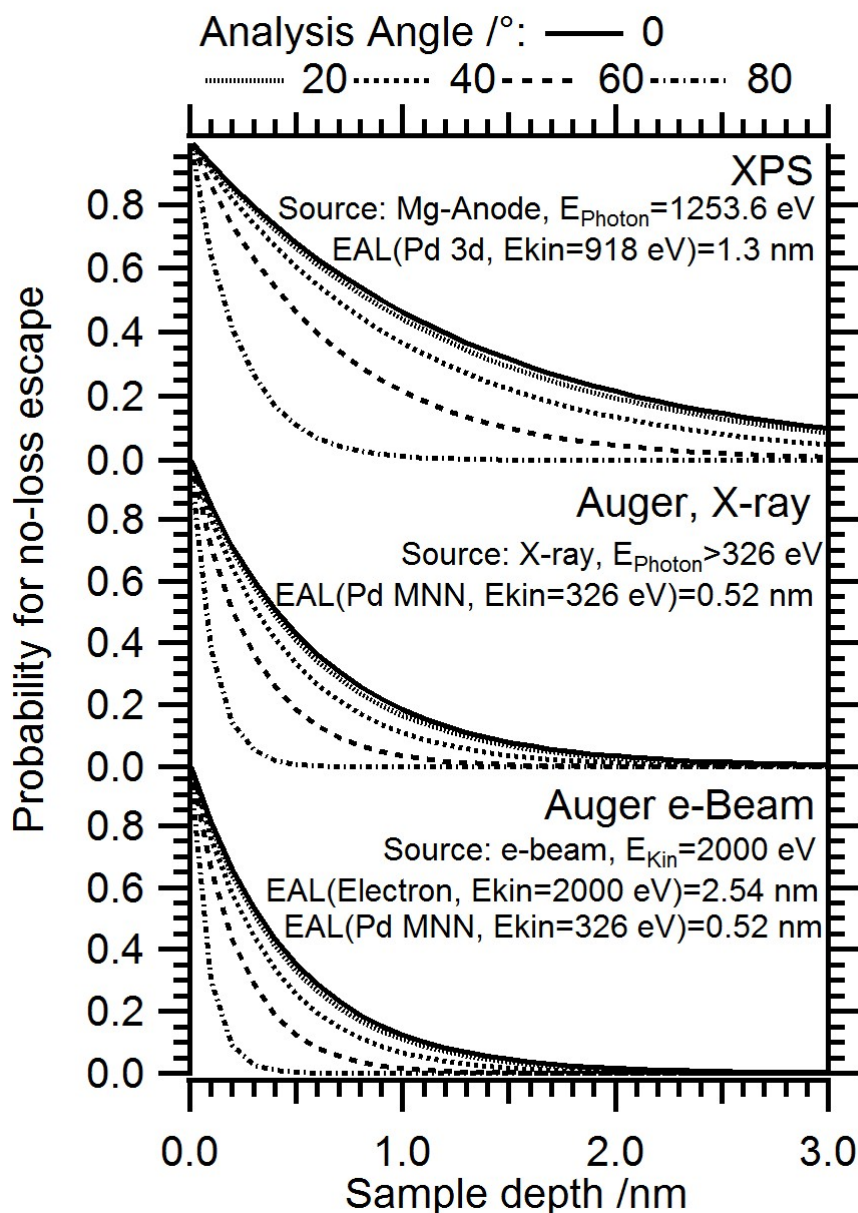
Figure 1: Depth-dependent probability of no-loss escapes of photoelectrons for XPS and AES (excitation with X-ray or e⁻ beam) measurements for different analysis angles between sample and spectrometer.

The attached, differentially pumped evaporators allow the preparation of real and inverse model catalysts. Differential pumping allows the exchange of evaporators without venting the whole UHV apparatus. Using the sample holder design shown in Figure 3, both sides of the catalyst (usually a thin metal or oxide-coated foil) are available for preparation, and hence, the active surface area can be doubled (~8 cm^2) in order to increase the catalytic turnover. For

accurate catalytic measurements it is necessary that both sides of the sample are prepared in the same way, otherwise the catalytic activity of front and backside would be different and hence, would lead to different results. After sample preparation and characterization, the catalyst can be transferred into the high-pressure reaction cell. Due to the quartz glass design of the catalyst reactor and due to the special quartz sample holder design shown in Figure 2, with no metal wires or supports connected to the catalyst sample, undesired catalytic activity of any of the reactor constituents can be avoided. The batch reactor has a separate gas analysing system (GC with EID/MS detector) for on-line monitoring of changes in the gas composition within the reactor, either by intermittent on-column injection of a sample loop or by continuous gas phase analysis via a defined capillary leak into the EID detector. This allows obtaining reaction rates and selectivity patterns. Due to the small reactor volume (296 ml) even small activities can be measured accurately and reproducibly. To demonstrate the specific strengths of the UHV-HP reaction setup, we show comparative results of methanol steam reforming on representative PdGa and PdZn near-surface intermetallic phases. The aim is to demonstrate the full potential of the UHV-HP catalysis system in obtaining structure-selectivity correlations through three-dimensional near-surface "pre-"catalyst characterization and subsequent catalytic testing.

B. UHV chamber

The original UHV setup, as described in ref.[16], was completely overhauled and the upper half of the UHV vessel (Trinos Vakuum-Systeme GmbH) exchanged by a new chamber with additional ports for upgraded and complementary spectroscopic and UHV equipment. A scheme of the new stainless steel UHV-system is shown in Figure 2. The main chamber (Vacuum Generators) has a volume of approximately 250 liters and is pumped by a turbo-molecular pump (Leybold-Heraeus, Turbovac) with roughing pump (Leybold-Heraeus, Trivac

B), an ion getter pump (Varian, Medivac) and a titanium sublimation pump (Vacuum Generators). The base pressure is in the 10^{-10} mbar range and recovers very fast (~30 min), even after exposures up to 10^{-5} mbar. For sample handling, a (xyzφ) manipulator with long z travel (250 mm) is placed off centre on top of the UHV-chamber. The setup has three levels as indicated by the numbers 1, 2, 3 in Figure 2, lower panel (side view).

The first level (1) is designed for spectroscopic sample analysis, catalytic testing and transfer to the high-pressure cell or to the load-lock. Reading the top view representation of Figure 2 in a clockwise manner, it is equipped with an 8 inch view port (a), a sputter gun (Vacuum Generators) (b), the transfer port and gate valve that separates the UHV-chamber from the high pressure catalysis cell (c), a fine-focus ion gun (Omicron, ISE 100) (d), a hemispherical analyser (Thermo Fischer, Alpha 110) (e) with a laterally (eccentrically) attached electron gun (Kimball Physics Inc., EFG-7) (f), an X-ray gun with alumina and magnesia anode (SPECS, XR 50) on a linear motion drive (g), the 1000 mm magnetically coupled linear transfer rod that is attached via an adjustable metal bellow (h) and the load lock (i), which is described in detail in the next section.

The second level (2) is designed for catalyst preparation. On the back side of the chamber below the ion and X-ray gun the two evaporators are placed at an angle of 90°. On the opposite side a quartz microbalance (Sycon, STM-100) is mounted on a linear motion drive which can be placed at the exact sample position for measurement of the evaporation rate. A U-shaped and water cooled copper block holds two quartz crystals, each facing one of the evaporators. On the left front side a home-built electron bombardment heater is mounted via a linear motion drive. Four helical thoriated tungsten filaments are spot welded on a tantalum frame that is held by two copper rods. An additional shield focuses the electrons onto the sample. For achieving very high temperatures (>1200 K) the sample can be additionally set to

an acceleration voltage of up to 700 V (usually ~ 400 V). The contamination of the sample with tungsten form the filaments was excluded by XPS.

The third and lowest level (3) is equipped with two Bayard-Alpert gauges (Granville-Philips and Balzers), a gas-dosing unit with high-precision leak valves for O_2, Ar, and H_2 dosing, a quadrupol mass spectrometer for gas analysis (Balzers, QME 125) and a shutter for shielding of the evaporators.

The load lock (i) was designed to facilitate the exchange of samples without the need to vent the whole UHV-chamber. Behind a gate valve (j) a sample holder mounted to a 500 mm magnetically coupled linear transfer rod is attached via a CF DN40 T-piece. The stainless steel sample holder of the load lock is designed with 7 places (machined slots) for samples and can therefore also be used as a sample storage unit (Figure 2, right part). The samples are loaded into the holder via the T-piece. The load lock is equipped via a metal bellow with a turbomolecular pump (Pfeiffer TC110) and a roughing pump (Pfeiffer DUO 1.5A), providing a base pressure in the low 10^{-7} mbar range. For pressure measurement a cold cathode ionization gauge (Leybold-Heraeus) is attached. For the sample transfer from the load lock to the UHV-chamber the gate valve is opened and the sample is positioned via the linear transfer below the UHV-sample holder. With a hook on the sample holder entering a 2.5 mm diameter drilled hole in the sample, the sample can be picked up afterwards (compare description of sample geometry in section B). The transfer procedure is described in section D. The pressure in the UHV-chamber is not exceeding the low 10^{-8} mbar range during the sample transfer.

Two ports in the middle section of the UHV-chamber (2) are equipped with evaporation sources. On the right port a home built evaporator is mounted on a linear motion drive. Due to difficulties in thermal evaporation of some materials (i.e. metallic Zr or refractory oxides like YSZ or ZrO_2), a home-built sputter source[17] is in use for sample preparation. On the left port, an additional gate valve with differential pumping makes a fast exchange of different evaporators possible without a bake-out of the main chamber. For differential pumping the

same pumping stage as for the load lock is used. Beside commercial micro-evaporators (TecTra) a home-built e$^-$-beam evaporator for high-power experiments is used. Especially the deposition of larger amounts of metallic gallium (liquid above 300 K, boiling point 2673 K) required a custom-made design of the evaporation source.
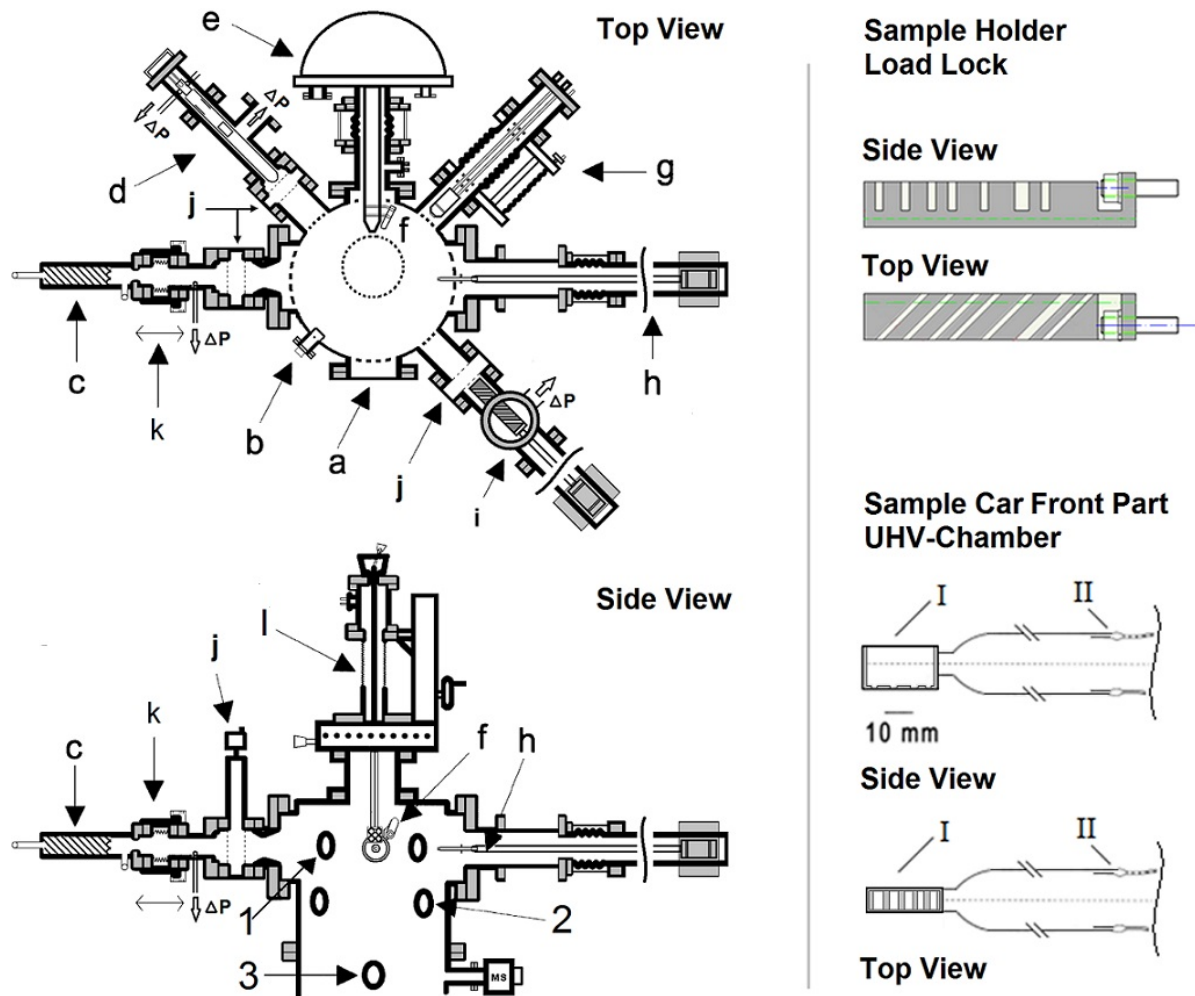

Figure 2: Left part: Schematic cross section of the UHV-chamber with the attached high-pressure cell in side and top view: (a) 8 inch viewport, (b) sputter gun, (c) quartz glass reactor, (d) ion gun for LEIS with differential pumping, (e) hemispherical analyser, (f) electron gun, (g) X-ray gun on linear motion drive, (h) transfer rod for sample transfer into the reactor, (i) load lock with differential pumping, (j) gate valves, (k) transfer port with differential pumping line and reactor seal, (l) xyzφ manipulator. (1) Level for sample testing, characterisation and transfer to high-pressure reaction cell. (2) Level for sample preparation with evaporators,

10

quartz microbalance and electron bombardment heater. (3) Level with gas dosing unit, Bayard-Alpert gauges and mass spectrometer. Right part: Side and top view of the sample holder of the load lock and schematic drawing of the front part of the sample car with catalyst holder (I) and the glass-to-metal seal (II).

The all-quartz sample car (Figure 2, bottom right) is also used as a catalyst holder for the catalytic reactions in the high pressure cell. As sample car we define the all-quartz front part up to the glass to metal seal of the transfer unit. On the front end a new catalyst holder is mounted (I). It has the shape of an open slot with perforated bottom enabling a better gas circulation. The height of the side walls is kept as low as possible, just to prevent the sample from falling out. The slot is held by a tubular quartz glass cylinder with a length of ~200 mm which ends in a quartz-to-metal seal (II). The tubular design (replacement body of the outer reactor wall) minimizes the volume of the reactor. All glass parts are made of quartz glass in order to perform high temperature catalysis up to 1000°C. The quartz-to-metal seal is welded to a stainless steel cylinder which is the main part of the transfer unit. The transfer unit itself and its mechanism is described in detail in reference[16], section II C.

C. UHV sample holder

The main sample holder of the UHV-chamber has a special design to meet the unique requirements of sample handling, preparation and transfer. Firstly, the sample has to be accessible for preparation on both sides to double the catalytic surface area. Secondly, the sample cannot have any permanent connections as wires, etc. because of the transfer procedure to the sample car and to the sample holder of the load lock. Thirdly, the sample needs to be insulated from the main chamber for current measurements during sputter cycles.

The connection to the measurement port is used to ground the sample for XPS, AES and LEIS measurements. The sample temperature is measured indirectly at one of the tantalum clips that hold the sample (figure 3, c). The offset between real and measured temperature was calibrated by a second thermocouple spot welded to a tantalum sample.

Figure 3 schematically shows the main components of the sample holder and the holding mechanism via the hook and the tantalum clips. By lowering the hook and entering it into the drilled 2.5 mm hole in the model catalyst the sample can be picked up. When the hook is retracted towards the sample holder the sample slides into the tantalum clips which hold the sample in place (Figure 3, side view). A more detailed description of the sample holder and its mechanism is already provided in figure 2 in reference[16].
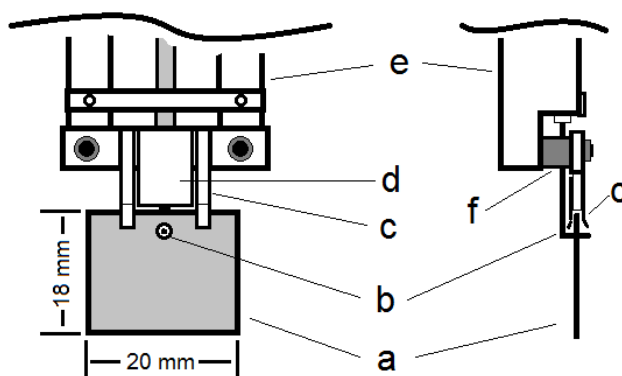

Figure 3: Schematic drawing of the sample holder and its mechanism in front (left) and side (right) view: (a) model catalyst, (b) hook to hold and pick up sample, (c) tantalum clips for sample holding, (d) support plate, (e) sample holder main body and (f) ceramics to electrically separate the sample from UHV chamber.

D. Description of sample transfers

The transfer and locking mechanism was not changed since the original setup and is technically described in ref.[16] section C and D. For the sake of understanding, a brief

summary is added at this stage. For the sample transfer from the UHV-chamber to the catalytic testing reactor, the catalyst holder of the sample car is positioned below the UHV-sample holder. Then the sample is moved downwards into the quartz slot and the hook is lowered until the foil is separated from the tantalum clips. By moving the manipulator backwards to move the hook out of the orifice in the sample, the foil is fully disconnected from the UHV-holder. Afterwards the sample car is moved into the reaction cell via the open transfer port with help of the linear transfer rod. After inserting the bayonet locking/sealing mechanism of the sample car into its seat inside the transfer port (as illustrated in reference[16], section E), the linear transfer rod can be retracted after unlocking by a half clockwise turn. Thereafter, the transfer port is sealed by mechanically pressing the sealing ring between the sample car and the reactor flange into its seats by a thread-driven linear motion drive (see ref.[16], Figure 4), and the UHV-chamber is separated from the reaction cell. During the whole transfer procedure the port is differentially pumped and the pressure in the UHV-chamber does not exceed the low 10^{-8} mbar range. To retract the catalyst back to the UHV chamber after catalytic testing, the reaction cell is first pumped down by a roughing pump to approximately 10^{-2} mbar, thereafter evacuated down to 10^{-8} mbar via differential pumping of the sealing mechanism and then the transfer steps are performed in reverse sequence.

For transfer of samples into or out of the UHV-chamber the load lock is used. First the sample is positioned in the sample holder of the load lock. After the load lock is pumped to the low 10^{-7} mbar range by a turbomolecular pump the gate valve is opened. The sample holder of the load lock is positioned below the UHV-sample holder. By lowering the manipulator, the hook is positioned behind the hole in the sample. By moving forward, the hook is inserted into the hole and by raising the hook upwards against the UHV-sample holder, the sample is fixed into the tantalum clips. Then the sample holder of the load lock can be retracted and the gate is closed. The pressure does not exceed the low 10^{-8} mbar range during this procedure. For transferring samples out of the UHV-chamber the procedure is performed in reverse order.

E. Catalytic reaction cell and gas analysis

Figure 4 shows a scheme of the catalytic reactor, the gas source unit and the gas detection setup. The high-pressure reaction cell is made of fused-quartz glass surrounded by a cylindrical furnace (Nabertherm P330), that allows accessing temperature ranges from 300 K to 1423 K. The temperature sensor of the furnace is located in between the reactor and the inner heating surface of the furnace. An all-metal re-circulating bellows pump is connected via 3 mm steel capillaries to the catalyst reactor forming a re-circulating batch system. The metal-to-quartz connections are arranged outside the furnace to avoid hot metal parts. The whole circulation system has a volume of 296 ml and is equipped with a pirani gauge. A glass bulb is connected to the system for dosing vapours of liquid reactants. The gas circulation has a connection to a roughing pump. After catalytic reactions the gas mixture can be pumped off and the catalyst is transferred back to the UHV-chamber for post-reaction characterization. A glass capillary leads directly from the high pressure reaction cell to the mass spectrometer of the gas chromatograph (GC-MS, Hewlett Packard G1800A GCD System) for continuous gas analysis. A steel capillary with a restrictor (needle valve) connects the circulation system to a second mass spectrometer (Balzers, QMA 125, Faraday Cup). The installation of the second mass spectrometer was necessary because the EID-MS detector is unable to detect hydrogen . For reactions where hydrogen is formed, both mass spectrometers are operated simultaneously. Additionally, the exact static gas composition can be determined at any point by injection of a defined gas volume sample loop of 200 μl into the column of the gas chromatograph.

The gas source unit (left side of Figure 4) is pumped directly by a roughing pump (Balzers, DUO 2.5 A) and allows the preparation of specific starting gas mixtures in a 0.6 l glass bulb.

Afterwards, the gas can be introduced to the reactor cell via a manifold. The pressure in the reactor for catalytic testing can be set between 0.2 mbar and 1500 mbar.
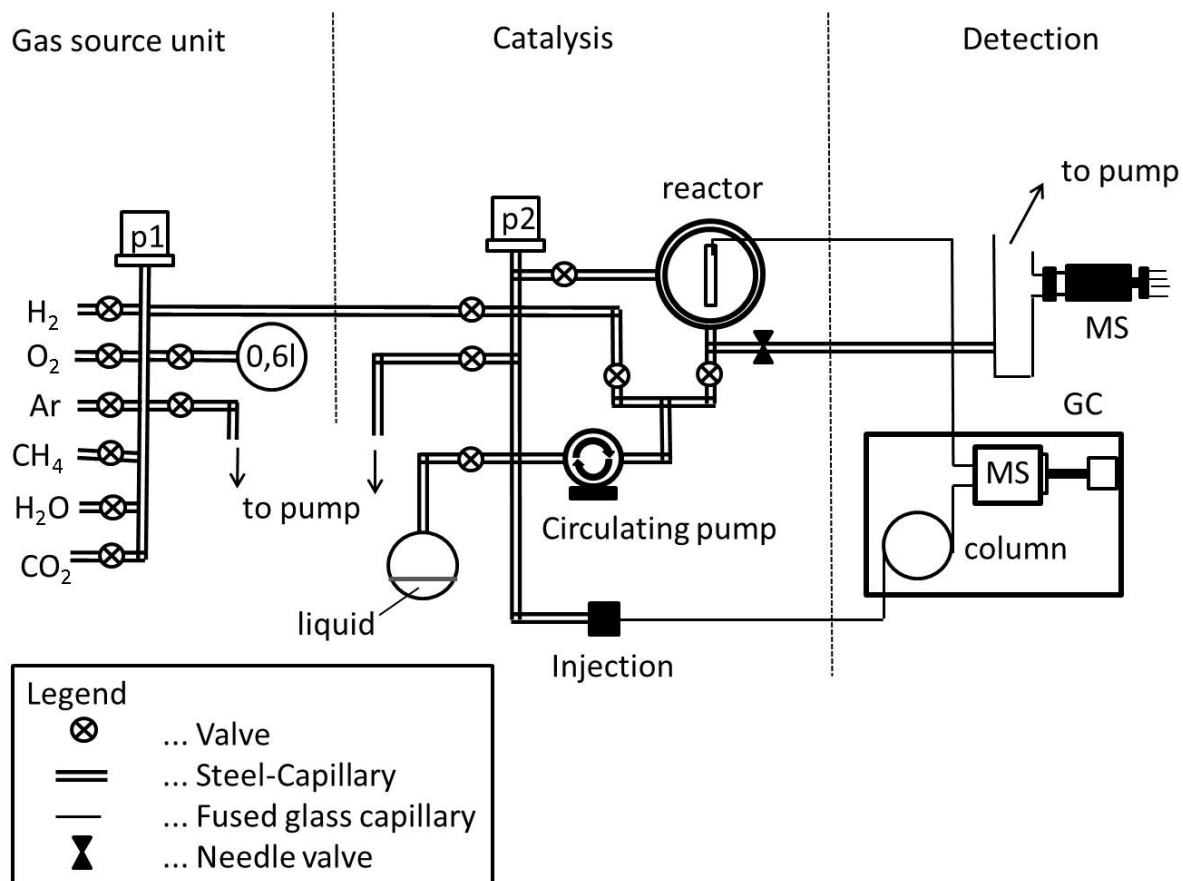

Figure 4: Schematic setup of the high pressure catalytic reactor, the gas source unit and the gas detection.

Application of the UHV-setup and high pressure reaction cell: Experimental results

The performance and capability of the described UHV system is demonstrated for the case of methanol steam reforming (MSR) on PdZn and PdGa near-surface intermetallic phases (NSIP). Besides the most prominent and industrially used $Cu/ZnO/Al_2O_3$ steam reforming catalyst[18], which suffers from undesired sintering at MSR reaction temperatures, a wide

variety of supported catalyst systems (PdZn/ZnO, PdIn/In$_2$O$_3$, Pd$_2$Ga/Ga$_2$O$_3$, PtZn/ZnO, PtGa/Ga$_2$O$_3$, NiZn/Zn, among others)[19] were studied by various groups to overcome the problem of long-term and high temperature stability of the industrial Cu/ZnO/Al$_2$O$_3$ methanol synthesis catalyst during MSR. As PdZn/ZnO, PdIn/In$_2$O$_3$, Pd$_2$Ga/Ga$_2$O$_3$ are promising CO$_2$-selective systems, as has been shown in previous studies[20-22], our research was focused on a detailed near-surface depth-resolved bimetallic model catalyst characterization, to reveal the electronic and geometric requirements of the intermetallic (near) surface regions for CO$_2$-selective methanol steam reforming. Comparative results for MSR on the PdZn and PdGa intermetallic near surface phases (NSIP) will be shown.

For preparation of the two different model catalysts, 3-4 ML of the respective metal (Zn for PdZn or Ga for PdGa) metal was deposited at 298 K to a pre-cleaned Pd foil. After annealing to 503 K, a 6-8 ML thick PdZn or PdGa surface intermetallic phase was formed on the Pd foil with a 1:1 composition[15, 23]. To gain insight into the thermal stability and the surface and near surface composition of the two different intermetallic phases, these toplayers were stepwise annealed to 870 K. The formation of the surface intermetallic phase was followed by AES and LEIS spectroscopy (Figure 5 and 6). For maximum surface sensitivity, LEIS measurements were performed with 1 kV He$^+$ ions, hence giving information about the atomic composition of the first atomic layer. Furthermore, by using He$^+$ with low kinetic energy, the inherent sputter effect of the LEIS measurements was suppressed by keeping the ion flux and the measurement time as low as possible. For information from deeper layers of the model systems, AES and XPS measurements were performed. Furthermore, XPS depth profiles could be obtained by varying the angle between sample and hemispherical analyser, revealing the 3-dimensional structure of the sample. These laboratory experiments were complemented by additional synchrotron radiation experiments with tuneable photon energy for obtaining XPS depth profiles (at beamline ISISS/HZB-Bessy II). Hence, information from different

sample depths was gained to additionally substantiate the depth distribution of the bimetallic dopants.
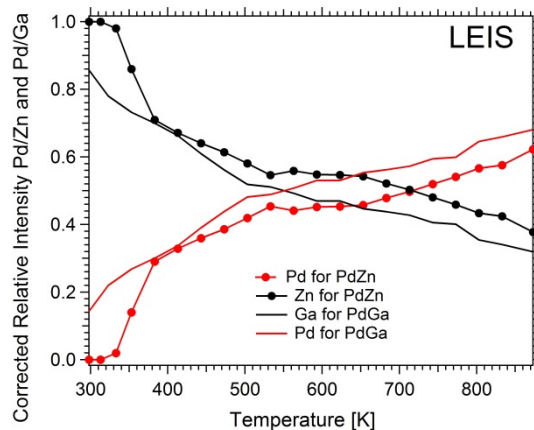

Figure 5: LEIS spectra (1 kV He$^+$) obtained on a Pd foil with deposition of 4 ML of Zn or Ga followed by subsequent heating to higher temperatures to induce the formation of a near-surface intermetallic phase.
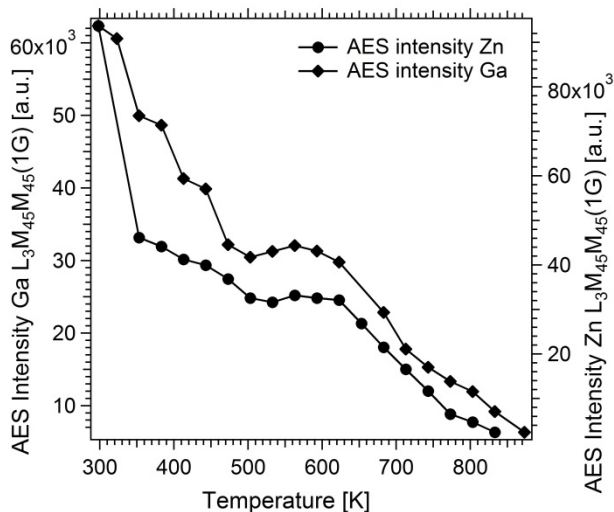

Figure 6: AES spectra obtained on Pd foil after deposition of 4 ML of Zn or Ga followed by subsequent heating to higher temperatures to induce the formation of a near-surface intermetallic phase.

From the surface composition derived from LEIS measurements in Figure 5, it is clear that in the case of PdZn, the Pd foil is initially fully covered by at least one "pure" Zn layer. With increasing temperature, the intermetallic phase formation (intermixing of Zn and Pd at the surface) sets in and the Zn-Pd ratio reaches a plateau region at ~530 K. From ~530 K to ~630 K a nearly constant ~1:1 surface composition is evident (only a slight change in the Pd:Zn ratio in figure 5 is observed). At temperatures above 630 K, the surface is depleted by Zn diffusion into the bulk and the ratio between Pd and Zn accordingly changes. For PdGa, already upon deposition at 298 K partial formation of a Ga-rich intermetallic phase can be observed. With increasing temperature, the intermetallic phase formation continues, until it also reaches a 1:1 composition of Pd:Ga at ~500 K. No pronounced plateau region is visible in the LEIS measurements. In contrast, a gradual compositional change towards a more Pd-rich surface is visible with increasing temperatures.

The comparison of the AES measurements with the LEIS results shows a similar trend for the low annealing temperatures for the two NSIP models PdZn and PdGa. For PdZn the intermetallic phase formation followed by a plateau region between ~500 K -~620 K can be observed. Also for PdGa the intermetallic phase formation monitored by AES is in line with the LEIS results. In the case of PdZn, annealing temperatures above 620 K lead to different results in AES and LEIS. Whereas in LEIS a very slow Zn-dilution of the surface layer can be observed (0.5 to 0.4 Pd/Zn ratio, between 623 K and 873 K), the AES Zn signal decreases much stronger with increasing annealing temperature (intensity decrease from ~3×10^4 to ~ 6×10^3 counts in the same temperature-range). This indicates that the Zn concentration in the first few subsurface layers drops much faster than the Zn content in the surface layer. These results lead to a model were at higher temperatures the 1:1 PdZn intermetallic phase depletes faster in Zn in the subsurface layers whereas the surface layer initially stays at the 1:1 composition and only at high temperatures the surface-located Zn is wandering into the Pd

bulk. From this we can conclude that above 630 K the formation of a one monolayer PdZn intermetallic surface phase occurs where one layer of Pd:Zn with a ~1:1 composition remains on top of the model catalyst.

For PdGa the comparison of the spectroscopic AES and LEIS results implicate a somewhat different behaviour. Whereas in LEIS no clear plateau region is visible between 500 K and 630 K, the AES results in Figure 6 indeed show a pronounced plateau region. The surface of the intermetallic phase gradually depletes in Ga with increasing annealing temperature, but the overall stoichiometry in the first 3-4 layers stays constant between 500 K and 630 K as it is evident from the AES measurements. At higher temperatures T > 623 K), both AES and LEIS show a gradual depletion of Ga of the model system. Again, surface depletion is less pronounced than subsurface depletion, in analogy to PdZn.

In combination with XPS and with additional information from impact-collision ion-scattering spectroscopy (ICISS, measured by W. Stadlmayr et al.[24]), a detailed picture of the two model catalysts could be achieved. Figure 7 highlights a schematic result for PdZn, where a pronounced corrugation of the surface with Zn outward and Pd inward is shown. This corrugation only occurs when the intermetallic compound has a sufficient thickness of several monolayers (ML). In comparison, for PdGa no preferential corrugation of the surface occurs.
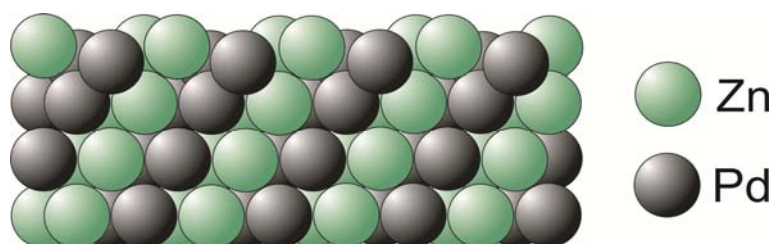

Figure 7: Schematic side view of the PdZn near surface intermetallic phase.

For the catalytic testing of the PdZn and PdGa model systems, the reactor was initially filled with 12 mbar of methanol and 24 mbar of water vapour. Besides 30 mbar of Ar as internal standard, 970 mbar of He were added as inert gas for better heat transfer and circulation in the

batch reactor. The reactor was heated with a linear ramp (9 K/minute) from 298 K to 623 K and was subsequently held isothermally at 623 K for 30 min. During the catalytic testing the gas composition was monitored continuously by EID/MS. Due to the constant removal of gas from the reactor through the gas capillary into the mass spectrometer, the gas pressure in the reactor is decreasing. The heating ramp of the furnace and therefore the increase of the temperature in the reactor lead to an increase of pressure. These two effects superimpose each other and make the analysis of absolute reaction rates and selectivities imprecise. To overcome this problem, for each catalytic reaction a defined amount of a reference gas (argon) is added and then all pressures can be normalised to the reference signal.

The catalytic results are shown in Figure 8. For PdGa the undesired CO formation sets in at ~540 K and has a maximum rate of ~0.23 mbar/min at 623 K. Simultaneously the formation of formaldehyde sets in with a maximum rate of ~0.006 mbar/min. At ~540 K the CO_2 formation rises with a maximum rate of 0.004 mbar/min. In the isothermal part of the reaction the catalytic activity decreases again due to deactivation processes. The active sites of the catalyst are blocked by carbon deposition and CO-poisoning[23]. Furthermore, the catalyst undergoes structural changes during the reaction. Due to the lack of the water activating ability of the PdGa 1:1 intermetallic phase, no pronounced CO_2 selectivity can be observed. Methanol is mainly dehydrogenated to CO and in contrast to pure Pd, the formation of formaldehyde is favoured as can be seen by the, in relation to the CO_2 formation rate, high formaldehyde formation rate. The same applies to unsupported Pd-rich Pd_2Ga samples[25]. In contrast, a supported Pd_2Ga intermetallic compound on Ga_2O_3 catalyst is highly active and selective as has been shown by Lorenz et al.[22, 26]. By comparison of the PdGa near surface intermetallic phase with Ga_2O_3-supported PdGa compounds, as e.g. studied by Lorenz et al.[22], the importance of the (bi-)metal-oxide contact area could be directly demonstrated.
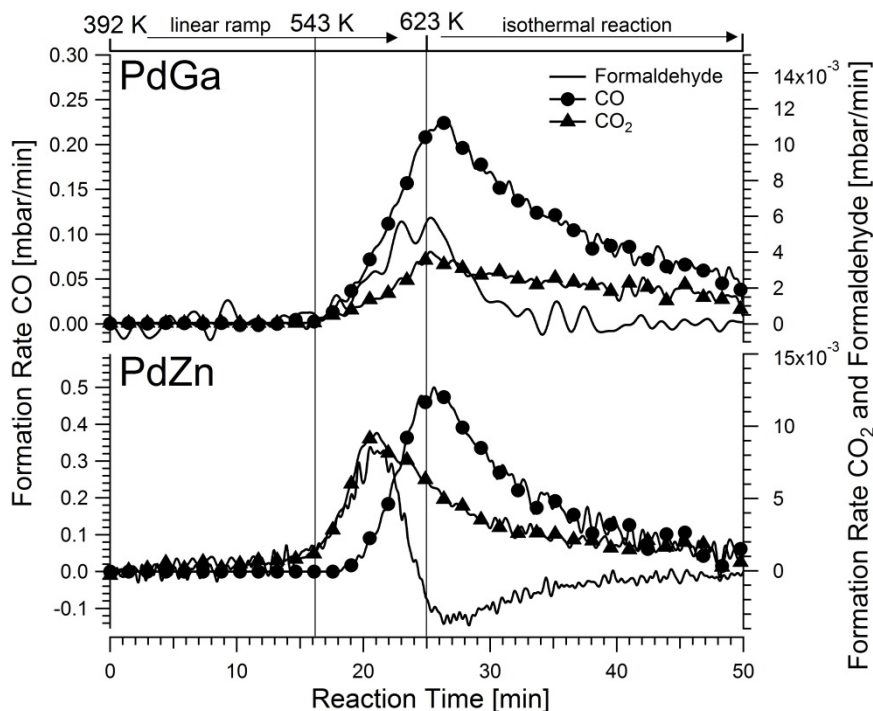
Figure 8: Temperature programmed methanol steam reforming reaction on a 1:1 Pd:Ga and Pd:Zn intermetallic phase (8 ML) prepared on a Pd foil. The initial pressure was 12 mbar methanol, 24 mbar water, 30 mbar Ar and 1000 mbar He. The temperature was increased by a linear ramp of 9 K/min from 298 K to 623 K followed by an isothermal reaction at 623 K.

In comparison to PdGa, a thicker, "multilayered" PdZn intermetallic surface phase is highly active and CO_2-selective in the methanol steam reforming reaction in a certain temperature range. Figure 8 (lower part) shows the results for MSR on the PdZn 1:1 intermetallic surface phase. Parallel CO_2 and formaldehyde formation can be observed starting at ~520 K with a maximum rate of ~0.01 mbar/min. At temperatures above 554 K the CO formation sets in reaching a maximum rate at 623 K of ~0.5 mbar/min. The strongly bonded CO and likely, also coking on the surface leads to deactivation of the catalyst in the isothermal part of the reaction. The corrugated 1:1 PdZn intermetallic surface phase provides the ability of water activation that is crucial for a highly active and selective steam reforming catalyst. In the

temperature range of 543 K – 573 K, the CO_2-selective MSR reaction is prevalent, but above 573 K, the selectivity changes towards CO because the catalyst undergoes structural changes. The initial corrugated surface with Zn outward/Pd inward changes to a flattened surface due to progressive subsurface located Zn diffusion into the bulk. This has been shown in detail in reference[15].

As the resolved near-surface catalyst characterization prior and after catalytic reactions without any contact to air is a prerequisite to understand the full catalytic properties of the entire catalyst system, Figure 9 exemplarily shows the capabilities of the UHV-HP system for depth analysis by angle-resolved photoelectron spectroscopy for a PdGa near-surface intermetallic phase. Together with catalytic results, but especially with equally depth-sensitive ambient pressure in-situ (operando) XPS measurements with varying photon energy at dedicated synchrotron facilities, a clear picture by means of valence band spectroscopy of the geometric dopant distribution and (electronic) structure of catalysts under working conditions evolves.

Generally, by changing the angle between the catalyst sample and the hemispherical analyser, the analysis depth of the XPS measurements can be varied[27]. The larger the angle between the analyser and the sample, the more surface sensitive the measurement. With this setup, three-dimensional information can be obtained and subsequently, information from both surface and bulk composition can be accordingly separated.

To demonstrate angle-resolved XPS on our apparatus, 4 ML of Ga were deposited on a Pd foil at 298 K. Subsequently, the sample was exposed to oxygen (200 mbar) at 298 K for 20 minutes leading to oxidation of the gallium on the surface. For the angle-resolved XPS measurements, the Pd 3d, Ga 3d and O 1s signal were recorded with a Mg Kα source at 6 different angles starting from 0° (most bulk sensitive), 18°, 38°, 54°, 64°, 80° (most surface sensitive) (see the supplementary material[28]). The acceptance angle of the hemispherical electron analyzer is +/- 1° for angle resolved measurements. The results in Figure 9 show for

surface sensitive measurements a higher Ga content (38% at 80°), that is slightly decreasing with analysing depth (31% at 0°). The oxygen content stays nearly the same for all angles. The Pd signal shows an increase with deeper analysis depth, from 6% at 80° (surface) to 11% at 0° (bulk). These results show that the surface layers are enriched by Ga. From the corresponding Ga 3d and Pd 3d spectra in the supporting information (figure 1) it can be seen that Ga-oxide (~20.8 eV) and Ga-metal (~18.9 eV) is present whereas for Pd 3d only the metallic compound (~336.3 eV) is detected. These observations lead to the conclusion that Ga oxidation parallel to partial PdGa intermetallic phase formation can be observed and a gradient in the Pd content in the surface layers is visible. The Ga-oxide is evenly distributed within the characterized surface layers.
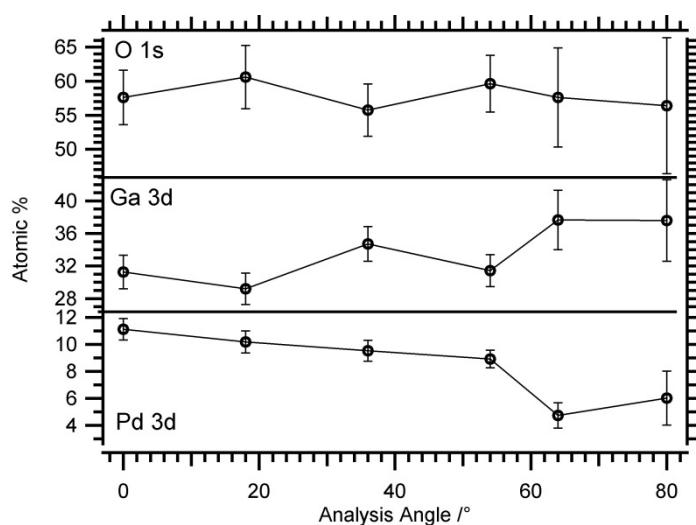

Figure 9: Surface composition of a Pd foil with a deposition of 4 ML Ga obtained by angle-resolved XPS measurements of the O 1s, Pd 3d and Ga 3d signal. With increasing angle, the measurements are more surface sensitive (0° most bulk sensitive, 80° most surface sensitive).

Conclusion

23

The scientific capabilities of the combined UHV characterization and the high-pressure catalysis approach have been exemplified by comparative studies of CO_2-selective methanol steam reforming on a PdGa and a PdZn 1:1 intermetallic phase. Prior to and after the catalytic measurements, detailed depth-resolved near-surface characterization of the electronic and geometric properties of the catalyst with XPS, AES and LEIS was carried out, greatly facilitated by the use of different analysis techniques with different information depth. We note, that only due to the sophisticated setup, the structural and catalytic requirements for CO_2-selective steam reforming on PdZn and PdGa intermetallic phases could be successully elucidated. The discussed scientific approach can in principle extended to any metal, intermetallic or oxide-supported system of catalytic relevance.

Acknowledgement

Reference

1.   G. Ertl, H. Knözinger, F. Schüth, J. Weitkamp, Handbook of Heterogeneous Catalysis, 8 Volumes.(Wiley, 2008).

2.   M. Che, J. C. Védrine, Characterization of Solid Materials and Heterogeneous Catalysts: From Structure to Surface Reactivity. (John Wiley & Sons, Incorporated, 2012).

3.   C. T. Campbell, J. C. Sharp, Y. X. Yao, E. M. Karp and T. L. Silbaugh, *Faraday Discussions* **152**, 227 (2011).

4.   F. Gao, D. W. Goodman, in *Annual Review of Physical Chemistry*, Vol 63, edited by M. A. Johnson, T. J. Martinez (*Annual Reviews*, Palo Alto, 2012), **63**, 265 (2012).

5.   H. J. Freund, N. Nilius, T. Risse, S. Schauermann, T. Schmidt, *Chemphyschem* **12**, 79 (2011).

6.   S. Zafeiratos, S. Piccinin, D. Teschner, *Catalysis Science & Technology* **2**, 1787 (2012).

7.   M. C. Xu, H. Noei, K. Fink, M. Muhler, Y. M. Wang, C. Woll, *Angewandte Chemie-International Edition* **51**, 4731 (2012).

8.   G. A. Somorjai, *Catalysis Today* **12**, 343 (1992).

9.   K. Hayek, M. Fuchs, B. Kotzer, W. Reichl, G. Rupprechter, *Topics in Catalysis* **13**, 55 (2000).

10.   D. W. Goodman, *Chemical Reviews* **95**, 523 (1995).

11.   G. Ertl, *Angewandte Chemie-International Edition* **29**, 1219 (1990).

12.   C. Mager-Maury, G. Bonnard, C. Chizallet, P. Sautet, P. Raybaud, *Chemcatchem* **3**, 200 (2011).

13.   D. R. Ou, T. Mori, H. Togasaki, M. Takahashi, F. Ye, J. Drennan, *Langmuir* **27**, 3859 (2011).

14.   C. Rameshan, W. Stadlmayr, S. Penner, H. Lorenz, N. Memmel, M. Havecker, R. Blume, D. Teschner, T. Rocha, D. Zemlyanov, A. Knop-Gericke, R. Schlogl, B. Klotzer, *Angewandte Chemie-International Edition* **51**, 3002 (2012).

15.   C. Rameshan, W. Stadlmayr, C. Weilach, S. Penner, H. Lorenz, M. Havecker, R. Blume, T. Rocha, D. Teschner, A. Knop-Gericke, R. Schlogl, N. Memmel, D. Zemlyanov, G. Rupprechter, B. Klotzer, *Angewandte Chemie-International Edition* **49**, 3224 (2010).

16.   W. Reichl, G. Rosina, G. Rupprechter, C. Zimmermann, K. Hayek, *Review of Scientific Instruments* **71**, 1495 (2000).

17.   L. Mayr, N. Koepfle, A. Auer, B. Kloetzer, S. Penner, *Review of Scientific Instruments* **84**, 94103 (2013).

18.   C. J. Jiang, D. L. Trimm, M. S. Wainwright, N. W. Cant, *Applied Catalysis A-General* **93**, 245 (1993).

19.   N. Iwasa, T. Mayanagi, N. Ogawa, K. Sakata, N. Takezawa, *Catalysis Letters* **54**, 119 (1998).

20.   C. Rameshan, C. Weilach, W. Stadlmayr, S. Penner, H. Lorenz, M. Hävecker, R. Blume, T. Rocha, D. Teschner, A. Knop-Gericke, R. Schlögl, D. Zemlyanov, N. Memmel, G. Rupprechter, B. Klötzer, *Journal of Catalysi*s **276**, 101 (2010).

21.   S. Sa, H. Silva, L. Brandao, J. M. Sousa, A. Mendes, *Applied Catalysis B-Environmental* **99**, 43 (2010).

22.   H. Lorenz, S. Penner, W. Jochum, C. Rameshan, B. Klotzer, *Applied Catalysis A-General* **358**, 203 (2009).

23.   C. Rameshan, W. Stadlmayr, S. Penner, H. Lorenz, L. Mayr, M. Haevecker, R. Blume, T. Rocha, D. Teschner, A. Knop-Gericke, R. Schloegl, D. Zemlyanov, N. Memmel, B. Kloetzer, *Journal of Catalysis* **290**, 126 (2012).

24.   W. Stadlmayr, C. Rameshan, C. Weilach, H. Lorenz, M. Havecker, R. Blume, T. Rocha, D. Teschner, A. Knop-Gericke, D. Zemlyanov, S. Penner, R. Schlogl, G. Rupprechter, B. Klotzer, N. Memmel, *Journal of Physical Chemistry C* **114**, 10850 (2010).

25.   M. Lukas, L. Harald, A. Marc, V. Sebastian, L. Yuan, C. Raul, B. Ulrich, Z. Dmitry, H. Michael, B. Raoul, K.-G. Axel, K. Bernhard, P. Simon, *Journal of Catalysis* **309**, 231 (2014).

26.   S. Penner, H. Lorenz, W. Jochum, M. Stoger-Pollach, D. Wang, C. Rameshan, B. Klotzer, *Applied Catalysis A-General* **358**, 193 (2009).

27.   P. J. Cumpson, *Journal of Electron Spectroscopy and Related Phenomena* **73**, 25 (1995).

28.   See supplementary material at [URL will be inserted by AIP] for the raw data of the angle dependent XPS measurements.